How to cite: *Angew. Chem. Int. Ed.* **2020**, *59*, 11399–11407
International Edition: doi.org/10.1002/anie.202003851
German Edition: doi.org/10.1002/ange.202003851

Three-Body Interactions | Hot Paper

Observation of the Low-Frequency Spectrum of the Water Trimer as a Sensitive Test of the Water-Trimer Potential and the Dipole-Moment Surface

*Raffael Schwan, Chen Qu, Devendra Mani, Nitish Pal, Gerhard Schwaab, Joel M. Bowman, Gregory S. Tschumper, and Martina Havenith**

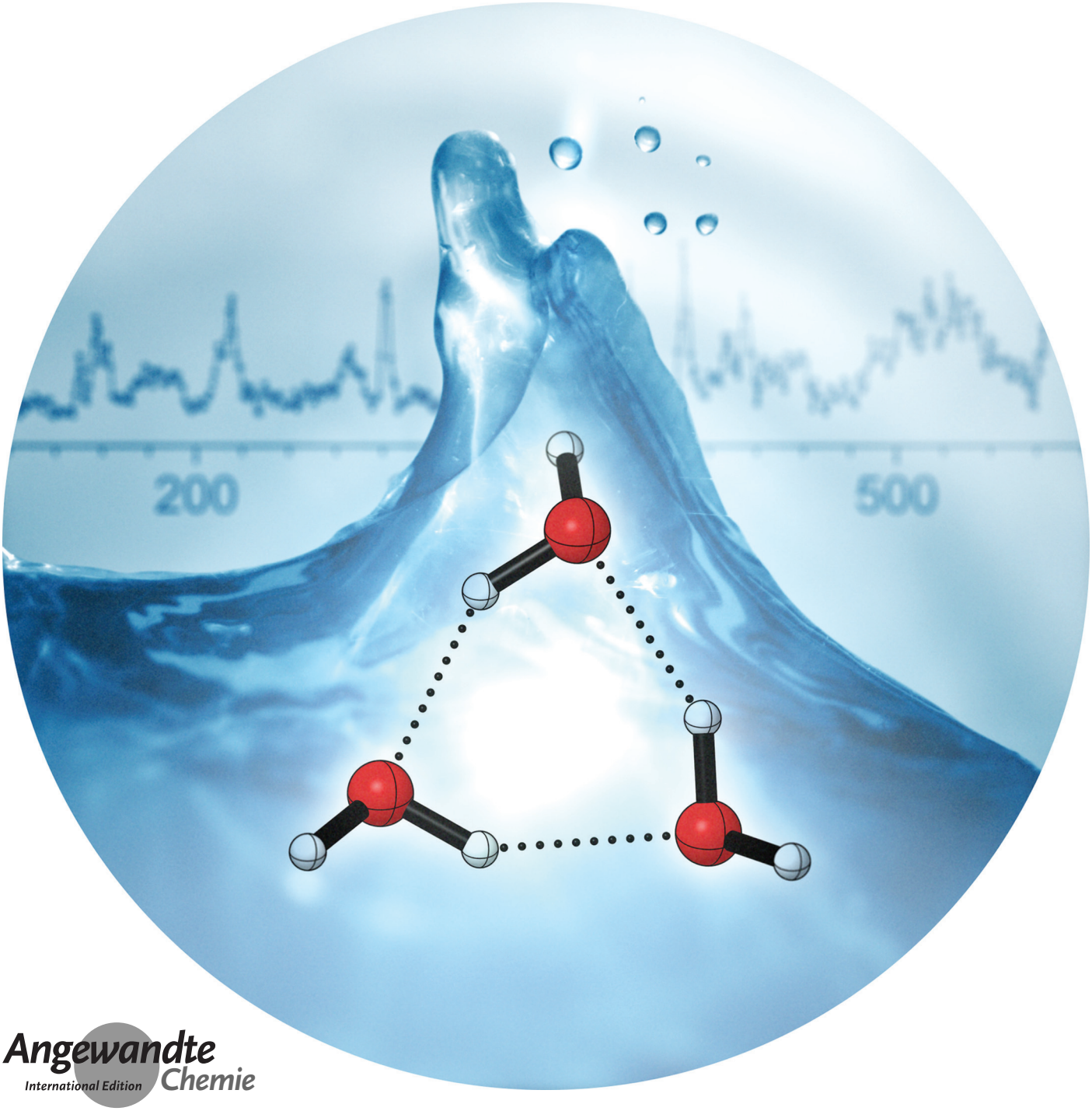

Abstract: *Intermolecular interactions in bulk water are dominated by pairwise and non-pairwise cooperative interactions. While accurate descriptions of the pairwise interactions are available and can be tested by precise low-frequency spectra of the water dimer up to 550 cm^{-1}, the same does not hold for the three-body interactions. Here, we report the first comprehensive spectrum of the water trimer in the frequency region from 70 to 620 cm^{-1} using helium-nanodroplet isolation and free-electron lasers. By comparison to accompanying high-level quantum calculations, the experimentally observed intermolecular bands can be assigned. The transition frequencies of the degenerate translation, the degenerate in-plane and the non-degenerate out-of-plane libration, as well as additional bands of the out-of-plane librational mode are reported for the first time. These provide a benchmark for state-of-the-art water potentials and dipole-moment surfaces, especially with respect to three-body interactions.*

Introduction

Water is the most prominent solvent and, therefore, of fundamental importance for chemistry and biology. However, despite decades of research, an accurate description of the underlying intermolecular interactions on a molecular level is still a scientific challenge. Spectroscopic studies, providing high-resolution spectra of intermolecular modes, in combination with ab-initio calculations give access to the potential energy surface (PES) of water clusters. An essential objective of this research is the development of a universal water model from first principles, which is capable to predict the properties of water in all its forms and over a wide range of conditions.[1–5]

The binding energy of water in the solid and liquid phase has been found to be dominated by two-body interactions.[6–8] While the water dimer is the ideal candidate to test the accuracy of the water potential for an accurate description of two-body interaction, the water trimer is the obvious candidate to test the three-body interactions, which are essential to accurately describe bulk water and ice. Initial studies focused on the accurate determination of an accurate water-dimer PES.[9–20] The cyclic equilibrium structure of the water trimer is significantly stabilized by three-body interactions, which will aid in incorporating cooperativity into the description of water models.

The many-body representation of the water potential has a long history, beginning with the seminal work of Stillinger and co-workers.[21] This representation for N water monomers can be written as

$$\sum_{i=1}^{N} V_i + \sum_{j>i}^{N}\sum_{i=1}^{N} V_{ij} + \sum_{k>j}^{N}\sum_{j>i}^{N}\sum_{i=1}^{N} V_{ijk} + \cdots, \quad (1)$$

where V_i is the one-body (monomer) potential of the ith monomer, V_{ij} is the two-body interaction between monomers i and j, V_{ijk} the three-body interaction between monomers i, j, k, etc. This representation is useful provided it converges quickly and ideally monotonically. This can be checked numerically by calculating the total electronic energy of N monomers, where, by necessity, N must be "small" and "small" is determined by the level of ab-initio theory used to obtain the electronic energy. For a high-level method such as CCSD(T), N is around 20. If we define the interaction energy as the total electronic energy minus the energy of the one-body monomers, these methods have shown that two-body terms account for roughly 90% of the interaction energy and the three-body terms account for roughly 8% of the remaining interaction energy. Thus, overall, the one-, two-, and three-body energies account for roughly 98% of the total energy.[8,22–24] Higher-body interactions, although small, matter for the energy ordering of isomeric forms of moderately sized water clusters. The small four- and higher-body interactions appear to be well represented by classical polarization effects.

Fully ab-initio approaches to obtain the two-body interactions for rigid monomers began with the CC-pol potential, which is a fit to thousands of CCSD(T) electronic energies.[2] For flexible monomers, the TTMn-F class of potentials was a major step in this direction. This potential used a sum of atom–atom exp-12 potentials to represent the full two-body (monomer) interactions with parameters fits to several hundred MP2 calculations. A fully ab-initio "non-parametric" approach was taken by Huang et al.,[25] who fit tens of thousands of CCSD(T)/aug-cc-pVTZ electronic energies for the water dimer using a fit basis of permutationally invariant polynomials (PIPs). This was already a significant challenge, as this potential is 12-dimensional (actually, 15 variables were used in the PIP fit). The latest version of this dimer potential[17] was used in a recent publication from the authors focused on the IR spectrum of the water dimer in the far-IR region.[26] The two-body interaction mentioned above is obtained from this dimer potential. Shortly after the work by Huang et al., a PIP fit was done for the water trimer based

[*] Dr. R. Schwan, Dr. D. Mani, N. Pal, Dr. G. Schwaab, Prof. M. Havenith
Physical Chemistry II, Department of Chemistry and Biochemistry, Ruhr-Universität Bochum
Bochum (Germany)
E-mail: martina.havenith@rub.de
Dr. C. Qu
Department of Chemistry Biochemistry, University of Maryland
College Park, MD 20742 (USA)
Prof. J. M. Bowman
Cherry L. Emerson Center for Scientific Computations and Department of Chemistry, Emory University
Atlanta, GA 30322 (USA)
Prof. G. S. Tschumper
Department of Chemistry and Biochemistry, University of Mississippi
University, MS 38677 (USA)
Supporting information and the ORCID identification number(s) for the author(s) of this article can be found under: https://doi.org/10.1002/anie.202003851.

on roughly 40000 MP2/aug-cc-pVTZ energies.[27] The three-body-interaction potential is obtained from this fit. In order to form an overall water potential, this three-body contribution was combined with three other components: the two-body interaction from the dimer potential, the spectroscopically accurate H_2O monomer potential of Partridge and Schwenke for the one-body contributions, and the long-range portion of the TTM3-F potential for four- and higher-body interactions. The result is referred to as the WHBB water potential.[28] Accurate dissociation energies of the water dimer and trimer were reported using WHBB as well as rigorous diffusion Monte-Carlo calculations of the zero-point energies. These energies were validated by experiment.[29,30] Of special significance to this paper was the determination that the intrinsic three-body interactions account for roughly 25% of the dissociation energy D_0.

An extensive review of ab-initio water potentials, with a focus on the MB-Pol potential, has recently appeared and the interested reader is referred there.[31] Clearly, it is important to test the quality of these ab-initio potentials. We do this here using new experiments on the far-IR spectrum of the water trimer, which provides a comprehensive overview of the intermolecular fingerprint range between 80 and 600 cm^{-1}. This is an extension of our recent work on the water dimer towards higher clusters.[26] The theoretical work consists of ab-initio VPT2 calculations of fundamental energies. Additionally, harmonic, scaled harmonic frequencies, and fixed-node diffusion Monte-Carlo (DMC) calculations of the splitting of the ground state are reported using the WHBB potential. Details of these calculations as well as harmonic frequencies obtained using the MB-Pol potential are given in the Supporting Information.

The water trimer has a cyclic equilibrium structure, with each water molecule serving as proton donor to one neighboring water molecule and as proton acceptor to the other.[32–39] In the equilibrium structure, two free hydrogen atoms are pointing upwards with respect to the O–O–O plane while the third is pointing downwards.[40] The equilibrium structure is thus denoted as {uud}.

The water-trimer vibrational spectrum consists of twelve intermolecular and nine intramolecular modes. The intermolecular modes are depicted in the Supporting Information. The spectrum is enriched by two low-barrier tunneling motions (see Figure 1a).[41–44] The molecular symmetry group of the cyclic equilibrium structure of water trimer is $C_1(M)$.[45] Proton interchange (without breaking any covalent bonds), results in 48 isoenergetic structures, which are connected via these two low-barrier tunneling pathways.

The first low-barrier tunneling pathway is denoted as flipping or torsional tunneling. Henceforth, we will refer to this tunneling pathway as torsional tunneling. Torsional tunneling changes the orientation of the free hydrogen atoms in the cyclic equilibrium structure of the water trimer (see Figure 1a). If torsional tunneling is feasible, the corresponding molecular-symmetry (MS) group is G_6, which is isomorphic to the C_{3h} point group. Tunneling will cause a splitting of each energy level into four (two non-degenerate and two degenerate) vibrational-tunneling levels labeled according to the irreducible representations in the G_6 MS group (see Figure 1b). A qualitative energy diagram is displayed in Figure 1c. The states are labeled by torsional quantum numbers $k = 0^0, \pm 1^0, \pm 2^0$, and 3^0. The irreducible representations are A_1, E_2, E_1, and A_2, respectively. The following transitions are allowed from the ground state: $A_2 \leftarrow A_1$ for parallel ($\Delta K = 0$) transitions and $E_1 \leftarrow A_1$ for perpendicular ($\Delta K = 1$) transitions, implying that their total angular quantum number changes by $\Delta|k-K| = 3$.[46] In the ground state, the torsional-tunneling splittings are β_t:$2\beta_t$:β_t, which is characteristic for a cyclic potential with six isoenergetic minima.[41] In the ground state, β_t was determined to be 21–22 cm^{-1}.[46–48]

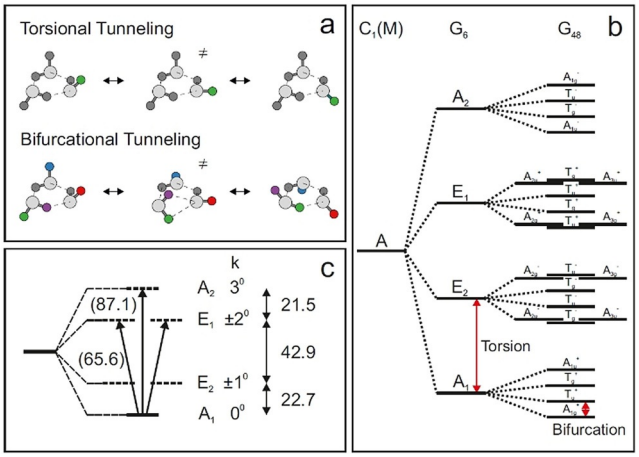

Figure 1. a) The two low-barrier-tunneling pathways of the water trimer. The torsional-tunneling pathway changes the orientation of the free hydrogen atoms and the bifurcation-tunneling pathway results in the exchange of the free and bound hydrogen atoms. b) Effect of the two low-barrier-tunneling pathways on the energy levels of the water trimer. Due to the torsional-tunneling pathway, each energy level is split into four energy levels labeled by the irreducible representations of the G_6 MS group. Due to the bifurcational-tunneling pathway, each energy level in the G_6 MS group is further split into four energy levels labeled by the irreducible representations of the G_{48} MS group. c) Manifold of the lowest torsional states $k = 0^0, \pm 1^0, \pm 2^0, 3^0$. Transitions originating in the $k = 0^0$ torsional state are indicated by solid arrows. Experimentally observed transition frequencies are shown next to the arrows. All values are given in cm^{-1}.

The second tunneling mode, the bifurcational tunneling, describes an exchange of the free and bound hydrogen atoms (see Figure 1a). The bifurcation-tunneling pathway results in a splitting of each energy level in the G_6 MS group into four levels, which are labeled by irreducible representations in the G_{48} MS group (see Figure 1b). In the ground state, this tunneling splitting is very small, that is, in the order of few MHz.[49]

The calculation of excited-state-tunneling splittings is a major challenge for theory. These must rely on a PES that accurately describes the large-amplitude motion connecting equivalent minima, and the saddle point (udp) separating them. At the saddle point, one free hydrogen atom is pointing upwards, one downwards, and one parallel with respect to the O–O–O plane. Fortunately, the WHBB PES describes this accurately, that is, the saddle-point energy is 83.2 cm^{-1}, in very good agreement with the benchmark value of 81.5 cm^{-1}.[50] To further test the accuracy of the WHBB PES for tunneling

splittings, we performed fixed-node diffusion DMC calculations of the splitting for the ground state (details are given in Supporting Information). The result of $26 \pm 5\ cm^{-1}$ is in good agreement with the experimental value of $\approx 22\ cm^{-1}$.[51] Unfortunately, the calculation of tunneling splittings for excited states using the DMC approach is not straightforward but could be the focus of future research.

Pioneering high-resolution gas-phase studies have been carried out by the Saykally group. Due to a lack of laser sources in the so-called THz gap, these studies predominantly focused on the frequency region below $100\ cm^{-1}$.[46–48,52–57] This region is dominated by a manifold of torsional states of the water trimer.[58] For the torsional modes, a harmonic approximation has been found to be inappropriate, and a pseudo-rotational model has been proposed.[40] These two low-barrier tunneling pathways are expected to couple strongly with the intermolecular modes of the water trimer, causing an anomalous tunneling pattern in the excited states. High-resolution studies of intermolecular modes have been restricted to few examples including the observation of the translational band of the $(D_2O)_3$ isotopologue at $142.8\ cm^{-1}$ and the out-of-plane librational band of the $(H_2O)_3$ isotopologue at approximately $520\ cm^{-1}$.[59–61]

Helium-nanodroplet-isolation spectroscopy is a versatile approach to infrared-spectroscopic investigations of molecules and molecular aggregates.[62–66] The technique enables stepwise aggregation and the spectroscopic characterization of molecular aggregates with well-defined cluster sizes at ultracold temperatures of 0.37 K.[67] Initially, the helium-nanodroplet-isolation technique was used to study the water monomer as well as small water clusters $(H_2O)_n$ with $n = 2$–6 in the region of the intramolecular O–H stretching mode[68–71] and the intramolecular H–O–H bending mode.[72] Most recently, we presented benchmark measurements of the low-frequency spectrum of the water dimer in helium nanodroplets in the frequency range from 50 to $500\ cm^{-1}$.[26]

Results and Discussion

Here, we report the first comprehensive low-frequency study of the water trimer including the translational mode (R_i), the in-plane librational modes (Φ_i), and the out-of-plane librational modes (β_i). The measurements were carried out using the BoHENDI helium-nanodroplet-isolation setup with the free-electron lasers at the FELIX laboratory in Nijmegen.[73]

In helium-nanodroplet-ionization (Hendi) spectroscopy, the absorption is measured indirectly as the depletion of the ion current of a certain ionic fragment in the mass spectrum upon excitation of the embedded solute. In the present study, we investigate water trimers which are formed after a sequential pickup of single water molecules. The depletion spectrum of small water clusters with an average pickup of 2–3 water molecules was recorded in the frequency region from 70 to $620\ cm^{-1}$ (see ref. [26] for details). Depletion was detected at $m/z = 19$, which was found to be highly selective for the water dimer as well as the water trimer.[72] Bands which were assigned to the water trimer were found in the following frequency range: 151–282 cm^{-1}, 313–317 cm^{-1}, 352–435 cm^{-1}, and 515–577 cm^{-1}.

In Figure 2, we display an overview of the recorded low-frequency spectrum of water clusters in helium nanodroplets in grey. Bands assigned to the translational mode (R_i), in-plane librational modes (Φ_i), and out-of-plane librational modes (β_i) are highlighted. A definitive assignment of the cluster size is based on pressure-dependent intensity measurements, so-called pickup curves. These were recorded at 86, 151, 158, 162, 185 210, 215, 266, 282, 313, 317, 352, 368, 386, 409, 428, 435, 515, 532, 570, and 577 cm^{-1}, and in case of the overlapping signals at 523 and 526 cm^{-1}, one pickup curve was measured at $524\ cm^{-1}$ (see the Supporting Information for details).

The pressure dependence of the signal at $86\ cm^{-1}$ follows a Poisson distribution with contributions from water dimers as well as water trimers.[26] The same ambiguity holds for the band at $185\ cm^{-1}$, which clearly shows contributions from several $(H_2O)_n$ clusters, with partial contributions of $n = 3$. Unfortunately, due to the low intensity of the signals at 231 and $249\ cm^{-1}$, we were unable to obtain conclusive pickup curves.

All transitions as observed before in high-resolution gas-phase studies of the Saykally group are shown as dashed lines.[46,47,59,60] In Figure 2b, lower trace, we display the predicted band center of our ab-initio calculations based on vibrational perturbation theory of second order (VPT2).

In the following, each intermolecular mode is assigned to a specific symmetry in G_6 (A_1, A_2, E_1, or E_2). Due to torsional tunneling, each intermolecular mode will split into four distinct states (see Figure 1 for the ground state). Our experimental frequency resolution is on the order of 0.5–$2\ cm^{-1}$, which is well below the torsional-tunneling splitting,

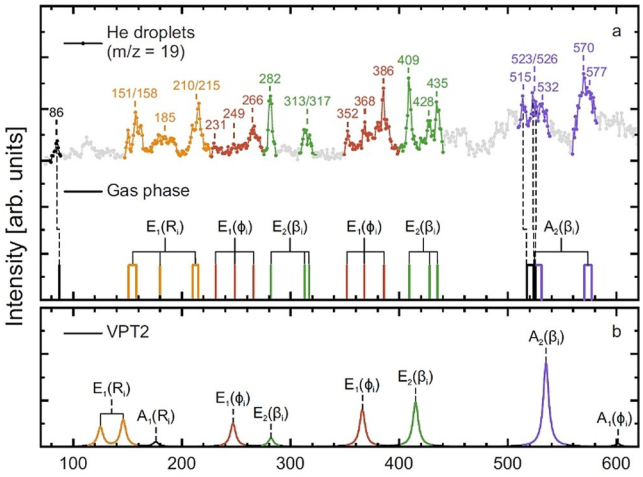

Figure 2. Comparison of our experimental FIR/THz water-trimer $(H_2O)_3$ spectrum (a, upper trace) with results from gas-phase studies[46,47,59,60] (a, lower trace) and results from VPT2 calculations (b). The band origins determined from the gas-phase studies are represented by black sticks, while those determined in the present study are shown as yellow, red, green, and violet sticks. Dashed lines indicate bands also observed in the gas-phase studies. In (b), each mode was assigned following the notation of the G_6 MS group as discussed in the text.

but exceeds the bifurcational tunneling splitting by far (a few MHz in the ground state). This implies that while we are able to resolve the torsional-tunneling splitting, the bifurcational splitting cannot be resolved, unless it is increased by several orders of magnitude upon vibrational excitation.

The water trimer is a symmetric-top molecule with gas-phase rotational constants of $A = B = 0.22$ and $C = 0.12\ cm^{-1}$.[46–48] Due to the helium environment, the rotational constants are expected to decrease by a factor of three.[66] Thus, distinct rotational transitions states cannot be resolved. At a temperature of 0.37 K, only the lowest torsional state ($k = 0^0$) is expected to be populated. Based on the transition rules, only parallel transitions ($\Delta K = 0$) from the lowest-populated $k = 0^0$ torsional state to states with overall vibrational-torsional A_2 symmetry or perpendicular transitions ($\Delta K = 1$) to states with an overall vibrational-torsional E_1 symmetry are allowed.

In our previous paper, we presented theoretical spectra for the water dimer. The most rigorous (and complex) theoretical spectrum came for fully-coupled quantum calculations using the WHBB potential and dipole-moment surfaces. Standard double harmonic calculations of the spectrum were also given, and this way, anharmonic/coupled-mode effects could be estimated by comparison of these two spectra. A simple scaling by a factor of 0.8 of the harmonic stick spectrum could be applied to bring the scaled spectrum into accord with the rigorous one. Assuming transferability to the trimer, we use that scaling factor here for the WHBB harmonic frequencies. Fortunately, new direct ab-initio VPT2 energies were also obtained for the trimer. These results are summarized in Table 1 along with experimental results. The intensities are taken from the double-harmonic calculations using the WHBB dipole-moment surface. A comparison of the WHBB harmonic frequencies given in this Table are compared with previous direct CCSDT:MP2/haQZ ones as well as MB-Pol ones (see the Supporting Information), and agreement is shown within a range of 0–10 cm^{-1}. In the following, we will use these predictions for an assignment of the observed bands.

Below 100 cm^{-1}, centered at 86 cm^{-1}, we observe one band, which is assigned to the $k = 3^0 \leftarrow 0^0$ perpendicular band in the ground state, in excellent agreement with results from gas-phase VRT studies, which yielded a band origin of 87.1 cm^{-1}.[46,47] The frequency range between 80 and 100 cm^{-1} is dominated by dimer lines at 86 cm^{-1} and at 99 cm^{-1}. The torsional band τ_1 is predicted at 101 cm^{-1} (see Table 1), but we were unable to observe this band.

In the frequency range between 100 and 220 cm^{-1}, we observed three new broad signals centered at 156, 185, and 213 cm^{-1}. The absorption peaks at 151/158 cm^{-1} and 210/215 cm^{-1} have a similar intensity and substructure; each one shows two overlapping peaks separated by 5/6 cm^{-1}. Based on comparison to the accompanying VPT2 calculations, we assign these to two perpendicular vibrational-tunneling transitions to the degenerate asymmetric translation modes $E_1(R_i)$ (Figure 3). Note that in the global minimum, only perpendicular transitions are allowed. At the {uud} stationary point, the transition dipole moment is expected to also have a parallel component, nevertheless, perpendicular transitions are predicted to be more intensive.

We attribute the splitting of 7 cm^{-1} between the bands at 151/158 cm^{-1} and the splitting of 5 cm^{-1} between the two bands of 210/215 cm^{-1} to a splitting of the previously degenerate $E_1(R_1)$ modes upon vibrational excitation. Based on our VPT2 calculations, these should be separated by 15 cm^{-1} (see Table 1). In a previous lower-level calculation by Klopper et al., a splitting of 7 cm^{-1} is predicted, in very good agreement with the experiment.[74]

The two perpendicular transitions of the $E_1(R_i)$ mode at 151/158 cm^{-1} and 210/215 cm^{-1} are separated by $3\beta_t$. Thus, based upon our experimental results, we deduce a torsional tunneling splitting of $\beta_t \approx 19/20\ cm^{-1}$, which agrees well with the torsional-tunneling splitting in the ground state. Based on this result, weaker parallel transitions are predicted around 170 to 180 cm^{-1}. These might contribute to the broad absorption centered around 185 cm^{-1}. Unfortunately, other bands as well as other water clusters also contribute to this band, which makes an unambiguous assignment for the band at 185 cm^{-1} impossible. Also, the $A_1(R_i)$ band at 185 cm^{-1}, which is predicted to have a small intensity, might contribute to the small broad peak at 185 cm^{-1}.

In the frequency region between 220 and 440 cm^{-1}, we observed peaks at 231, 249, 266, 282, 313, 317, 352, 368, 386, 409, 428, and 435 cm^{-1}. By comparison to our VPT2 calculation, we attribute these to transitions to the degenerate in-plane libration $E_1(\Phi_i)$ pre-

Table 1: Comparison of experimental results (cm^{-1}) with results from indicated calculations (cm^{-1}). Each mode at the {udu} global minimum is assigned to its symmetry in the G_6 MS group.

mode	*theory* harmonic[a]	scaled harmonic[b]	VPT2[c]	intensity	*exp. He nanodroplet* ν	β	*exp. gas phase*
$K = 3^0 \leftarrow 0^0$					86(⊥)	22[51]	87.1[46,47]
τ_1	166	128	101	22	–	–	–
$E_1(R_i)$	177	141	139	21	151(⊥)/210(⊥)	20	–
$E_1(R_i)$	185	148	154	29	158(⊥)/215(⊥)	19	–
τ_2	195	157	152	10	–		–
$A_1(R_i)$	215	172	175	8	185(?)		–
τ_3	234	184	185	5	–	–	–
$E_1(\Phi_i)$	332	268	266	25	266(⊥)		–
$E_2(\beta_i)$	345	276	282	9	282(⊥)/313,317 (⊥)		–
$E_1(\Phi_i)$	431	347	358	40	352/368/386		–
$E_2(\beta_i)$	551	448	416	48	409(⊥),428/435 (⊥)		–
$A_2(\beta_i)$	644	516	564	91	515,523,526,532 (∥) 570,577(⊥)	49	517.2, 523.9, 525.3[3]
$A_1(\Phi_i)$	833	662	670	3	–	–	–

[a, b] WHBB ref. [28]. [c] Present results.

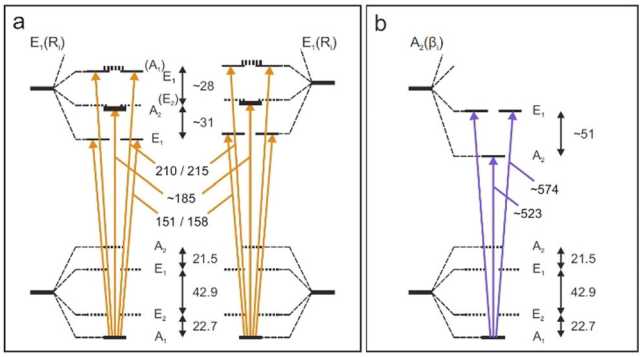

Figure 3. Qualitative energy-level diagrams for a) the degenerate translations $E_1(R_i)$ and b) the non-degenerate out-of-plane libration $A_2(\beta_i)$. Observed transitions are indicated by solid arrows along with the observed experimental frequencies. All values are given in cm^{-1}.

dicted at 267 and 359 cm^{-1}, and to the degenerate out-of-plane libration $E_2(\beta_i)$ predicted at 282 and 416 cm^{-1} (Figure 4). Note that in the present case, $E_1(\Phi_i)$ and $E_2(\beta_i)$ will mix at the {uud} stationary point. For the $E_1(\Phi_i)$ and $E_2(\beta_i)$ modes, two perpendicular vibrational-torsional transitions and one parallel transition are allowed; however, perpendicular transitions are predicted to have a higher intensities.

By comparison to our VPT2 calculations, we assign the peaks at 231/249/266 cm^{-1} and 352/368/386 cm^{-1} tentatively to transitions to the degenerate in-plane libration $E_1(\Phi_i)$. Both sets show a similar intensity pattern and are found in close proximity to the predicted band center. Although the peaks at 231/249 cm^{-1} are very small and do not allow an unambiguous cluster assignment, the signal at 266 cm^{-1} can clearly be attributed to $(H_2O)_3$. This peak is assigned to the perpendicular transition to the $E_1(\Phi_i)$ mode with an overall torsional vibrational symmetry of $E_1 \otimes E_1 = 2A_1 \oplus E_1$. The same holds for the intense peak at 386 cm^{-1}. Note that both states might be split into further overlapping peaks.

The peaks at 352 and 368 cm^{-1} are tentatively assigned to parallel and perpendicular transitions to the lower-lying torsional states of the in-plane libration $E_1(\Phi_i)$ mode, predicted at 358 cm^{-1}. Due to the strong mixing of $E_1(\Phi_i)$ and $E_2(\beta_i)$, we cannot anticipate a regular torsional-tunneling pattern. Therefore, we abstain from deducing a β_t value. Instead, we show the deduced energy-level diagram in Figure 4.

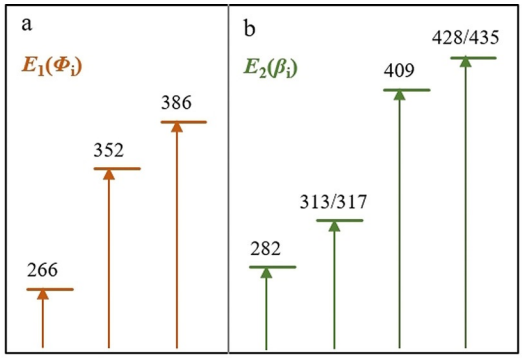

Figure 4. Qualitative energy-level diagrams for the observed torsional states of a) the split degenerate in-plane librations $E_1(\Phi_i)$ and b) the degenerate out-of-plane librations $E_2(\beta_i)$. Due to strong mixing between $E_1(\Phi_i)$ and $E_2(\beta_i)$, an unambiguous assignment is not possible, as discussed in the text.

In the same way, we assign the signals at 282 cm^{-1} and 313/317 cm^{-1} as well as 409 and 428/435 cm^{-1} to the four perpendicular transitions to the two degenerate out-of-plane librations $E_2(\beta_i)$. We speculate that the experimentally observed smaller splittings of 4 and 7 cm^{-1} can be attributed to an increased bifurcational-tunneling splitting upon vibrational excitation, similar as was proposed before for the out-of-plane $A_2(\beta_i)$ librational mode.[3]

In the frequency range above 500 cm^{-1}, two intermolecular modes are predicted based on our VPT2 calculations: the out-of-plane liberation $A_2(\beta_i)$ is predicted at 564 cm^{-1} and the in-plane librational mode $A_1(\Phi_i)$ at 673 cm^{-1}. Since the $A_1(\Phi_i)$ mode is expected to have an intensity thirty times smaller than the $A_2(\beta_i)$ band (see Table 1), we assign all peaks above 500 cm^{-1} to parallel and perpendicular transitions to the out-of-plane libration, $A_2(\beta_i)$.

The first three experimentally observed peaks at 515, 523/526, and 532 cm^{-1} are in excellent agreement with the previously observed band origins at 517.2, 523.9, and 525.3 cm^{-1} in a high-resolution gas-phase study.[3] These were tentatively assigned to parallel transition from the ground state to the $A_2(\beta_i)$ out-of-plane librational mode with a resolved bifurcational-tunneling splitting. The bifurcational splits in each state in a quartet are denoted as A_1^-,A_2^-, T_1^-, and T_2^-.[75] They attributed the splitting between the band centers at 517.2, 523.9, and 525.3 cm^{-1} to the bifurcational-tunneling splitting, implying that the latter is increased by three orders of magnitude upon librational excitation.[3]

We assign the peak at 532 cm^{-1} to the fourth bifurcational-tunneling component of the parallel transition to the out-of-plane libration (the A_1^+ subband), which has not been detected before. For transitions from $K'' = 0$, this fourth component of the quartet is expected to be a factor of 3, 9, and 11 smaller than each of the other components. However, if we sum over all K'' states (since we lack rotational resolution), their intensities become comparable.

In our study, we not only report the center frequency of the fourth tunneling component at 532 cm^{-1} for the first time, but we can state that the pattern is no longer equally spaced—as in the ground state. In the ground state, the bifurcational tunneling can be explained by a single flip arrangement with an excitation energy well below the tunneling barrier.[59,60] This approximation obviously does not hold any longer.

We also observed a second, broad band with a substructure centered at 570 and 577 cm^{-1} (see Figure 2). These peaks are assigned to perpendicular transitions to the intermolecular $A_2(\beta_i)$ mode, reported here for the first time. Previously, the bifurcational and the torsional splittings were postulated to be of the same order of magnitude (−3.1 and −2.3 cm^{-1}, or 1.6 and 4.6 cm^{-1}). Based on our study, we are now able to deduce the size of the torsional-tunneling splitting in the vibrational excited $A_2(\beta_i)$ mode. The difference between the center frequencies of parallel and perpendicular transitions in this mode amount to $\beta_t = 49$ cm^{-1}, which is one order of magnitude larger than the bifurcational-tunneling splitting

($\approx 8\ cm^{-1}$). β_t is increased by a factor of more than two compared to the ground state and thus larger than previously anticipated. The magnitude of the bifurcational tunneling in the vibrationally excited $A_2(\beta_i)$ mode can be deduced from the difference between the first and fourth component of the quartet, that is, the 517 cm^{-1} and 532 cm^{-1} peak: $2\beta_b = (532-517)\ cm^{-1}$; thus, $\beta_b = 8.5\ cm^{-1}$. We confirm that the bifurcation-tunneling splitting is increased by more than three orders of magnitude compared to the ground state, but $\beta_t > \beta_b$ still holds. Both tunneling motions, albeit to a different extent, are strongly coupled to the out-of-plane librational mode.

It should also be noted that the bifurcational-tunneling quartet is obviously more closely spaced in the perpendicular transition, observed between 570 and 577 cm^{-1}, than in the case of parallel transitions, observed between 515 and 532 cm^{-1}. In contrast, in the ground state, the observed splitting is the same for the parallel as well as the perpendicular transition. If the splitting is dominantly caused by the coupled single-flip bifuractional matrix elements, then we expect a splitting of $\beta_b = 8\beta_{1flb}$ for parallel transitions and $\beta_b = 4\beta_{1flb}$ in case of perpendicular transitions. The experimentally observed difference for parallel transitions amounts to 17 cm^{-1}. Hence, we deduce a value of $\beta_{1flb} = 2.125\ cm^{-1}$. The anticipated maximum splitting for perpendicular transitions would then amount to $4\beta_{1flb} = 8.5\ cm^{-1}$, which is—within our experimental uncertainty—in very good agreement with the experimentally observed splitting of $(577–570)\ cm^{-1} = 7\ cm^{-1}$.

To conclude this section, we describe calculations of the ground-vibrational-state tunneling splitting in the water trimer using the ring-polymer instanton (RPI) method.[76–78] These used the WHBB potential[76,78] and MB-Pol potential.[77] The calculated splitting of about 50 cm^{-1}, using either potential, is more than a factor of two larger than experiment. However, in recent work of Vaillant et al.,[77] a splitting of $(26 \pm 2)\ cm^{-1}$ was obtained using a more rigorous PIMD approach with the MB-Pol potential. This splitting is in very good agreement with the present DMC fixed-node splitting of $(26 \pm 5)\ cm^{-1}$ using WHBB, and both results are in good agreement with experiment. This indicates that these ab-initio potentials can be used to obtain accurate tunneling splittings, provided they are used with rigorous calculations of the splittings.

Conclusion

We report the first comprehensive FIR/THz spectrum of the water trimer in the frequency region from 80 to 600 cm^{-1}. Excellent agreement with previous high-resolution gas-phase studies, which were limited to the torsional mode τ_1 at 86 cm^{-1} and the librational mode around 520 cm^{-1}, show that the influence of the helium-nanodroplet environment can be neglected within our experimental resolution ($\approx 1\ cm^{-1}$), similar to what was observed before for the water dimer.[26]

Based on a comparison of the experimentally observed transitions with predictions from VPT2 calculations, we are able to assign the following intermolecular modes with partially resolved torsional- and even bifurcational-tunneling splitting: the degenerate translation $E_1(R_i)$, the non-degenerate out-of-plane libration $A_2(\beta_i)$, two degenerate in-plane librations $E_1(\Phi_i)$, and two degenerate out-of-plane librations $E_2(\beta_i)$. These energies provide an excellent test for any state-of-the-art water-trimer potential.

We note that the torsional-tunneling splitting is sensitive to the intermolecular excitation: For the degenerate translation $E_1(R_i)$ mode, the torsional-tunneling splitting amounts to 20 cm^{-1}, close to the value in the ground state. For the $A_2(\beta_i)$ mode above 500 cm^{-1}, the torsional-tunneling splitting has increased to 49 cm^{-1}. Due to the coupling of the $E_1(\Phi_i)$ and $E_2(\beta_i)$ modes, the torsional-tunneling pattern is affected, thus, we abstain from deducing a value for the torsional splitting β_t.

For the out-of-plane libration, we observe all components of the bifurcation-tunneling quartet and confirm the previously proposed increase in tunneling splitting by several orders of magnitude.[59,60] We tentatively assign the splitting in the degenerate out-of-plane libration $E_2(\beta_i)$ mode of 4 cm^{-1} (317–313) cm^{-1} and 7 cm^{-1} at (435–428) cm^{-1} to a bifurcational-tunneling splitting. The increase in bifurcational-tunneling splitting will depend on the actual tunneling path, that is, whether the intermolecular mode and the bifuractional-tunneling mode are strongly coupled (are along the same coordinate) and on the energy of excitation in comparison to the tunneling barrier.

When computing the projections of the {uud} normal modes onto the bifurcational mode, we find that both projections, for $E_2(\beta_i)$ as well as $E_1(R_1)$, are in the same order of magnitude as in case of the $A_2(\beta_i)$ mode (see the Supporting Information). While we can speculate that experimentally, at 386 cm^{-1}, also a substructure can be resolved, it is more prominent in case of the out-of-plane librations. This might indicate that the bifurcational-tunneling pathway involves an out-of-plane mode. The observed increase in bifurcation tunneling towards higher frequencies can be attributed to the higher vibrational-excitation energy, which results in an effective decrease of the tunneling barrier.

Up to now, torsional states of the water trimer have been treated with a three-dimensional model[58,79] which reproduces the energies of the torsional states with $k = 0$, 1, 2, and 3. However, to describe the manifold of torsional states for the translational and librational modes accurately, a treatment of the water trimer in a twelve-dimensional model (including all twelve intermolecular modes) is inevitable. This remains one of the challenges of future theoretical studies.

Acknowledgements

This work was funded by the Deutsche Forschungsgemeinschaft (DFG, German Research Foundation) under Germany's Excellence Strategy—EXC 2033–390677874—RESOLV. The FELIX laboratory is funded by the Stichting voor Fundamenteel Onderzoek der Materie (FOM) and LASER-LAB-EUROPE grant 654148. The theoretical work at Emory was supported by NASA, Grant No NNX16AF09G. The theoretical work at the University of Mississippi was carried out with support from the National Science Foundation under grant number CHE-1664998 and the computational resources

provided by the Mississippi Center for Supercomputing Research.

Conflict of interest

The authors declare no conflict of interest.

Keywords: helium nanodroplets · vibrational spectroscopy · water cluster · water potential

[1] N. Goldman, C. Leforestier, R. Saykally, *Philos. Trans. R. Soc. London Ser. A* **2005**, *363*, 493 – 508.
[2] R. Bukowski, K. Szalewicz, G. C. Groenenboom, A. Van der Avoird, *Science* **2007**, *315*, 1249 – 1252.
[3] V. Babin, C. Leforestier, F. Paesani, *J. Chem. Theory Comput.* **2013**, *9*, 5395 – 5403.
[4] V. Babin, G. R. Medders, F. Paesani, *J. Chem. Theory Comput.* **2014**, *10*, 1599 – 1607.
[5] G. R. Medders, V. Babin, F. Paesani, *J. Chem. Theory Comput.* **2014**, *10*, 2906 – 2910.
[6] S. S. Xantheas, *J. Chem. Phys.* **1994**, *100*, 7523 – 7534.
[7] J. K. Gregory, D. C. Clary, *J. Phys. Chem.* **1996**, *100*, 18014 – 18022.
[8] M. P. Hodges, A. J. Stone, S. S. Xantheas, *J. Phys. Chem. A* **1997**, *101*, 9163 – 9168.
[9] C. Millot, A. J. Stone, *Mol. Phys.* **1992**, *77*, 439 – 462.
[10] R. S. Fellers, C. Leforestier, L. Braly, M. Brown, R. Saykally, *Science* **1999**, *284*, 945 – 948.
[11] E. M. Mas, R. Bukowski, K. Szalewicz, G. C. Groenenboom, P. E. Wormer, A. van der Avoird, *J. Chem. Phys.* **2000**, *113*, 6687 – 6701.
[12] G. Groenenboom, P. Wormer, A. Van Der Avoird, E. Mas, R. Bukowski, K. Szalewicz, *J. Chem. Phys.* **2000**, *113*, 6702 – 6715.
[13] N. Goldman, R. Fellers, M. Brown, L. Braly, C. Keoshian, C. Leforestier, R. Saykally, *J. Chem. Phys.* **2002**, *116*, 10148 – 10163.
[14] C. Leforestier, F. Gatti, R. S. Fellers, R. J. Saykally, *J. Chem. Phys.* **2002**, *117*, 8710 – 8722.
[15] G. S. Tschumper, M. L. Leininger, B. C. Hoffman, E. F. Valeev, H. F. Schaefer III, M. Quack, *J. Chem. Phys.* **2002**, *116*, 690 – 701.
[16] X. Huang, B. J. Braams, J. M. Bowman, R. E. Kelly, J. Tennyson, G. C. Groenenboom, A. van der Avoird, *J. Chem. Phys.* **2008**, *128*, 034312.
[17] A. Shank, Y. Wang, A. Kaledin, B. J. Braams, J. M. Bowman, *J. Chem. Phys.* **2009**, *130*, 144314.
[18] R. E. Kelly, J. Tennyson, G. C. Groenenboom, A. van der Avoird, *J. Quant. Spectrosc. Radiat. Transfer* **2010**, *111*, 1262 – 1276.
[19] C. Leforestier, K. Szalewicz, A. Van Der Avoird, *J. Chem. Phys.* **2012**, *137*, 014305.
[20] C. Leforestier, *J. Chem. Phys.* **2014**, *140*, 074106.
[21] D. Hankins, J. Moskowitz, F. Stillinger, *J. Chem. Phys.* **1970**, *53*, 4544 – 4554.
[22] J. Cui, H. Liu, K. D. Jordan, *J. Phys. Chem. B* **2006**, *110*, 18872 – 18878.
[23] U. Góra, R. Podeszwa, W. Cencek, K. Szalewicz, *J. Chem. Phys.* **2011**, *135*, 224102.
[24] D. M. Bates, J. R. Smith, G. S. Tschumper, *J. Chem. Theory Comput.* **2011**, *7*, 2753 – 2760.
[25] X. Huang, B. J. Braams, J. M. Bowman, *J. Phys. Chem. A* **2006**, *110*, 445 – 451.
[26] R. Schwan, C. Qu, D. Mani, N. Pal, L. van der Meer, B. Redlich, C. Leforestier, J. M. Bowman, G. Schwaab, M. Havenith, *Angew. Chem. Int. Ed.* **2019**, *58*, 13119 – 13126; *Angew. Chem.* **2019**, *131*, 13253 – 13260.
[27] Y. Wang, B. C. Shepler, B. J. Braams, J. M. Bowman, *J. Chem. Phys.* **2009**, *131*, 054511.
[28] Y. Wang, X. Huang, B. C. Shepler, B. J. Braams, J. M. Bowman, *J. Chem. Phys.* **2011**, *134*, 094509.
[29] B. E. Rocher-Casterline, L. C. Ch'ng, A. K. Mollner, H. Reisler, *J. Chem. Phys.* **2011**, *134*, 211101.
[30] L. C. Ch'ng, A. K. Samanta, Y. Wang, J. M. Bowman, H. Reisler, *J. Phys. Chem. A* **2013**, *117*, 7207 – 7216.
[31] G. A. Cisneros, K. T. Wikfeldt, L. Ojamäe, J. Lu, Y. Xu, H. Torabifard, A. P. Bartok, G. Csanyi, V. Molinero, F. Paesani, *Chem. Rev.* **2016**, *116*, 7501 – 7528.
[32] A. J. Tursi, E. R. Nixon, *J. Chem. Phys.* **1970**, *52*, 1521 – 1528.
[33] T. R. Dyke, J. Muenter, *J. Chem. Phys.* **1972**, *57*, 5011 – 5012.
[34] L. Fredin, B. Nelander, G. Ribbegård, *J. Chem. Phys.* **1977**, *66*, 4065 – 4072.
[35] M. Vernon, D. Krajnovich, H. Kwok, J. Lisy, Y. Shen, Y.-T. Lee, *J. Chem. Phys.* **1982**, *77*, 47 – 57.
[36] R. H. Page, J. G. Frey, Y.-R. Shen, Y. T. Lee, *Chem. Phys. Lett.* **1984**, *106*, 373 – 376.
[37] D. Coker, R. Miller, R. Watts, *J. Chem. Phys.* **1985**, *82*, 3554 – 3562.
[38] Z. Huang, R. Miller, *J. Chem. Phys.* **1989**, *91*, 6613 – 6631.
[39] J. Paul, R. Provencal, C. Chapo, K. Roth, R. Casaes, R. Saykally, *J. Phys. Chem. A* **1999**, *103*, 2972 – 2974.
[40] M. Schütz, T. Bürgi, S. Leutwyler, H. B. Bürgi, *J. Chem. Phys.* **1993**, *99*, 5228 – 5238.
[41] D. J. Wales, *J. Am. Chem. Soc.* **1993**, *115*, 11180 – 11190.
[42] T. R. Walsh, D. J. Wales, *J. Chem. Soc. Faraday Trans.* **1996**, *92*, 2505 – 2517.
[43] A. van der Avoird, E. Olthof, P. Wormer, *J. Chem. Phys.* **1996**, *105*, 8034 – 8050.
[44] T. Taketsugu, D. J. Wales, *Mol. Phys.* **2002**, *100*, 2793 – 2806.
[45] H. C. Longuet-Higgins, *Mol. Phys.* **1963**, *6*, 445 – 460.
[46] E. Olthof, A. Van der Avoird, P. Wormer, K. Liu, R. Saykally, *J. Chem. Phys.* **1996**, *105*, 8051 – 8063.
[47] K. Liu, J. G. Loeser, M. J. Elrod, B. C. Host, J. Rzepiela, N. Pugliano, R. J. Saykally, *J. Am. Chem. Soc.* **1994**, *116*, 3507 – 3512.
[48] M. G. Brown, M. R. Viant, R. P. McLaughlin, C. J. Keoshian, E. Michael, J. D. Cruzan, R. J. Saykally, A. van der Avoird, *J. Chem. Phys.* **1999**, *111*, 7789 – 7800.
[49] F. N. Keutsch, L. B. Braly, M. G. Brown, H. A. Harker, P. B. Petersen, C. Leforestier, R. J. Saykally, *J. Chem. Phys.* **2003**, *119*, 8927 – 8937.
[50] J. A. Anderson, K. Crager, L. Fedoroff, G. S. Tschumper, *J. Chem. Phys.* **2004**, *121*, 11023 – 11029.
[51] F. N. Keutsch, J. D. Cruzan, R. J. Saykally, *Chem. Rev.* **2003**, *103*, 2533 – 2578.
[52] K. Liu, M. J. Elrod, J. G. Loeser, J. Cruzan, N. Pugliano, M. Brown, J. Rzepiela, R. J. Saykally, *Faraday Discuss.* **1994**, *97*, 35 – 41.
[53] S. Suzuki, G. A. Blake, *Chem. Phys. Lett.* **1994**, *229*, 499 – 505.
[54] M. R. Viant, J. D. Cruzan, D. D. Lucas, M. G. Brown, K. Liu, R. J. Saykally, *J. Phys. Chem. A* **1997**, *101*, 9032 – 9041.
[55] M. R. Viant, M. G. Brown, J. D. Cruzan, R. J. Saykally, M. Geleijns, A. van der Avoird, *J. Chem. Phys.* **1999**, *110*, 4369 – 4381.
[56] F. N. Keutsch, E. N. Karyakin, R. J. Saykally, A. van der Avoird, *J. Chem. Phys.* **2001**, *114*, 3988 – 3993.
[57] J.-x. Han, L. K. Takahashi, W. Lin, E. Lee, F. N. Keutsch, R. J. Saykally, *Chem. Phys. Lett.* **2006**, *423*, 344 – 351.
[58] D. Sabo, Z. Bačić, T. Bürgi, S. Leutwyler, *Chem. Phys. Lett.* **1995**, *244*, 283 – 294.
[59] F. N. Keutsch, R. S. Fellers, M. R. Viant, R. J. Saykally, *J. Chem. Phys.* **2001**, *114*, 4005 – 4015.

[60] F. N. Keutsch, R. S. Fellers, M. G. Brown, M. R. Viant, P. B. Petersen, R. J. Saykally, *J. Am. Chem. Soc.* **2001**, *123*, 5938 – 5941.
[61] F. N. Keutsch, M. G. Brown, P. B. Petersen, R. J. Saykally, M. Geleijns, A. Van Der Avoird, *J. Chem. Phys.* **2001**, *114*, 3994 – 4004.
[62] J. P. Toennies, A. F. Vilesov, *Annu. Rev. Phys. Chem.* **1998**, *49*, 1 – 41.
[63] C. Callegari, K. K. Lehmann, R. Schmied, G. Scoles, *J. Chem. Phys.* **2001**, *115*, 10090 – 10110.
[64] J. P. Toennies, A. F. Vilesov, *Angew. Chem. Int. Ed.* **2004**, *43*, 2622 – 2648; *Angew. Chem.* **2004**, *116*, 2674 – 2702.
[65] F. Stienkemeier, K. K. Lehmann, *J. Phys. B* **2006**, *39*, R127.
[66] M. Choi, G. Douberly, T. Falconer, W. Lewis, C. Lindsay, J. Merritt, P. Stiles, R. Miller, *Int. Rev. Phys. Chem.* **2006**, *25*, 15 – 75.
[67] M. Hartmann, R. Miller, J. Toennies, A. Vilesov, *Phys. Rev. Lett.* **1995**, *75*, 1566.
[68] C. J. Burnham, S. S. Xantheas, M. A. Miller, B. E. Applegate, R. E. Miller, *J. Chem. Phys.* **2002**, *117*, 1109 – 1122.
[69] C. Lindsay, G. Douberly, R. Miller, *J. Mol. Struct.* **2006**, *786*, 96 – 104.
[70] K. E. Kuyanov, M. N. Slipchenko, A. F. Vilesov, *Chem. Phys. Lett.* **2006**, *427*, 5 – 9.
[71] K. Kuyanov-Prozument, M. Y. Choi, A. F. Vilesov, *J. Chem. Phys.* **2010**, *132*, 014304.
[72] R. Schwan, M. Kaufmann, D. Leicht, G. Schwaab, M. Havenith, *Phys. Chem. Chem. Phys.* **2016**, *18*, 24063 – 24069.
[73] D. Mani, T. Fischer, R. Schwan, A. Dey, B. Redlich, A. Van Der Meer, G. Schwaab, M. Havenith, *RSC Adv.* **2017**, *7*, 54318 – 54325.
[74] W. Klopper, M. Schütz, H. P. Lüthi, S. Leutwyler, *J. Chem. Phys.* **1995**, *103*, 1085 – 1098.
[75] F. N. Keutsch, R. J. Saykally, D. J. Wales, *J. Chem. Phys.* **2002**, *117*, 8823 – 8835.
[76] J. O. Richardson, S. C. Althorpe, D. J. Wales, *J. Chem. Phys.* **2011**, *135*, 124109.
[77] C. L. Vaillant, D. J. Wales, S. C. Althorpe, *J. Phys. Chem. Lett.* **2019**, *10*, 7300 – 7304.
[78] M. Eraković, C. L. Vaillant, M. T. Cvitaš, *J. Chem. Phys.* **2020**, *152*, 084111.
[79] A. van der Avoird, K. Szalewicz, *J. Chem. Phys.* **2008**, *128*, 014302.

Manuscript received: March 15, 2020
Version of record online: May 28, 2020

